A method for the three-dimensional statistical shape analysis of the bony orbit

Hans Lamecker, Lukas Kamer, Antonia Wittmers, Stefan Zachow, Thomas Kaup, Alexander Schramm, Hansrudi Noser, Beat Hammer

Introduction. 2D CT or CBCT (Cone Beam CT) reconstructions are routinely used for the assessment and treatment of orbital fractures [1] and deformities. Routine 3D rendering of such image data is unreliable due to the conjunction of the so called partial volume effects during imaging and the very thin nature of the orbital walls.
However, 3D CT data have the potential to improve scientific shape analysis and radiological diagnostics as well as surgical planning and treatment. To be able to generate a precise 3D model of the orbit, manual or semi-automatic segmentation tools have to be employed. Automatic 3D reconstruction of the orbit would make 3D models more applicable for tasks such as generating virtual templates or for optimizing the shape of orbital implants.
We adapted a method for the 3D statistical assessment of normal orbital shape and its variability to accomplish automatic 3D reconstruction.

Methods. The main challenge for performing statistical analysis of three-dimensional shapes lies in the identification of corresponding points on the surfaces of different individual shapes. We adopt the method of consistent patch decomposition and parameterization [2] to solve this problem. All shapes are represented as triangulated surfaces, which are extracted semi-automatically from CT data sets. This *training data base* contains the normal variability of orbital shape to be analyzed. First, all surfaces are decomposed into a number of corresponding regions (= patches). Patch boundaries are constructed semi-automatically by specifying characteristic anatomical landmarks and connecting them along anatomically meaningful lines, e.g. ridges or crests. In a second step, corresponding regions are parameterized onto a common base domain under the constraint of minimizing metric distortion. The concatenation of the parameterizations allows furnishing all surfaces with the same topological triangle mesh, thereby providing explicit point correspondences densely across all shapes. Finally, all shapes can be represented mathematically in a common frame of reference and statistical analysis becomes possible. We employ principal component analysis to extract the most important variations within the training set. This information can be encoded within a statistical shape model, representing the flexible template of interest.
In order to develop and assess the method, CT data of 10 European Caucasians patients (4 female, 6 male, ages 17-74) with normal orbits are used. The data were obtained using routine CT head protocols on a standard multislice CT scanner (SOMATOM Sensation 10, Siemens AG, Erlangen, Germany), and consist of 0.5 mm axial sections with a high resolution bone window scan.

Results. Based on anatomical structures and enhanced visualisation methods we decompose the orbit into 6 regions (Fig. 3). The outer borderline of the patches correspond anatomically to the openings of the bony orbit: i.e. the orbital rim, the superior- and inferior orbital fissure, the orifice of the optic foramen, and the lacrimal fossa with the naso-lacrimal canal opening. All the borderlines of these structures are typically characterized by a pronounced curvature (see Fig. 2).
The largest patch (1) is formed by the roof of the orbital cavity. Laterally this patch is bounded by a line connecting the end of the superior orbital fissure to the orbital rim (i.e. to fronto-zygomatic suture). Medially three borderlines define the patch: the first from the optic canal to the superior orbital fissure, the second from the optic canal along the highest curvature, including the anterior and posterior ethmoidal foramina, to the posterior upper end or the lacrimal fossa. The third is delineated from patch 6 by high curvature. Patch 6 is triangle-shaped with the orbital rim as an anterior borderline. Inferiorly the lacrimal fossa forms a separate patch 5, again defined by high curvature. A small patch (4) delineates the naso-lacrimal canal opening. Patch 2 contains the lateral wall delimited by the shortest line between the end of the inferior orbital fissure and the orbital rim, and a short line at the inferior end of the orbital fissure forms the borderline to Patch 3. The latter consists of the medial wall and the orbital floor.

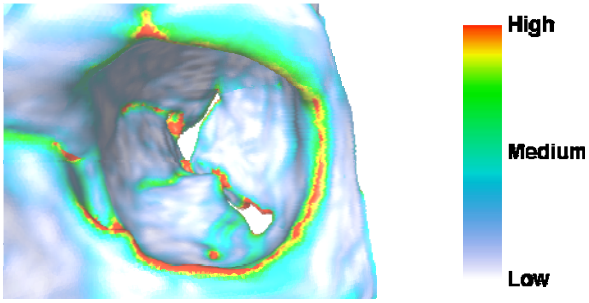

Figure 2. Curvature in the orbital region.

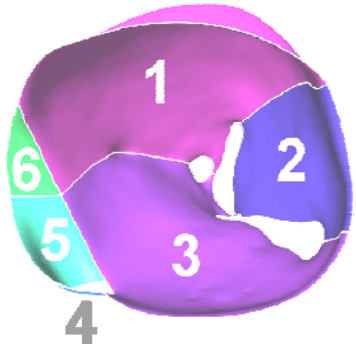

Figure 3. Patch decomposition of the left orbit. The average orbital shape derived from the training data is shown.

Based on these patches a statistical model of the left orbit of the training data set was computed. Fig. 3 shows the average orbital shape. The size of the training models has been normalized. In Fig. 4 the three main modes of variations are depicted (from left to right). Top and bottom row indicate the spectrum of variation contained in each mode respectively. Additionally, the normal deviation from the mean shape is colour-coded onto the surface. Furthermore, a leave-one-out test is performed to measure the quality of the statistical shape model. For each training shape, a statistical model is created that does not contain this specific shape. The remaining model is fitted to this shape by minimizing surface distance with respect to the model parameters. Results are shown in Fig. 5. The numbers indicate the accuracy of the shape model to represent any given arbitrary shape (generalization ability).

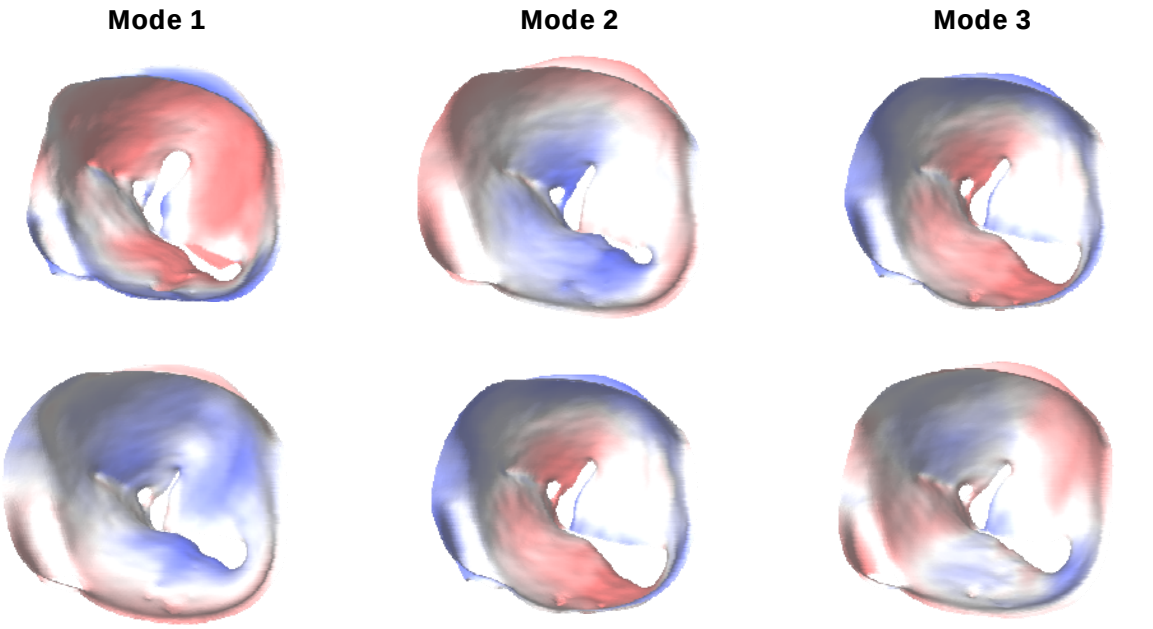

Figure 4. First three modes of variation with normal deviations from the mean shape (colors indicate deviations in mm)

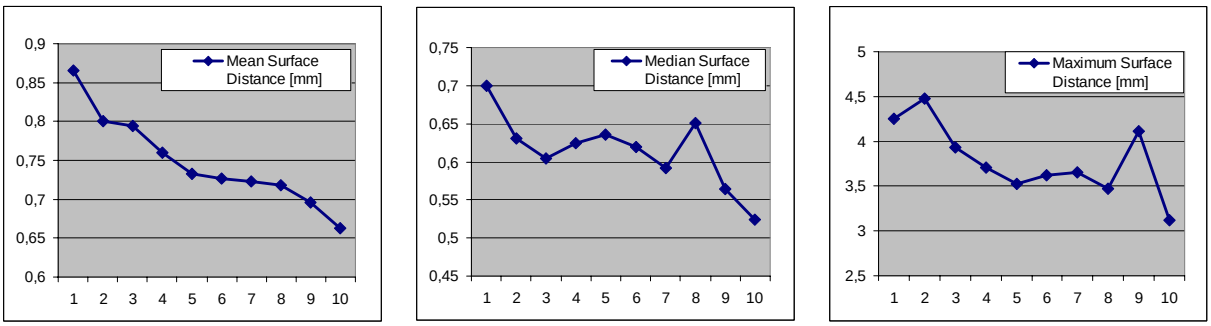

Figure 5. Results of leave-one-out test. The surface distances represent the errors in reconstructing 10 individual shapes (x-axis) with shape models made of 9 training data sets.

Discussion. This method is well suited to generate a statistical model of the complex shape of the orbit because it offers the possibility to subdivide it into meaningful anatomical regions with well-defined transitions thus solving well the correspondence problem. Besides quantitative description of shape variation, it offers the possibility to visualize in 3D the complete shape space of the training set. It offers a wide range of potential applications such as shape analysis of larger samples (differences between: right/left orbits, ages, gender, ethnic groups, etc.), implant optimization, rapid prototyping (Fig. 6) as well as surgical planning and treatment [3].

However, in routine clinical practice, automated processing including 3D visualisation of the individual orbital shape remains a difficult task. Individual anatomical shape variations may not be distinguished from pathological shape alteration. The correct shape reconstruction from image data is further complicated by partial volume effects.

References.

[1] Hammer B. Orbital fractures: Diagnosis, operative treatment, secondary corrections. Hogrefe & Huber Publishers, Seattle, Toronto, Bern, Göttingen, 1995.
[2] H. Lamecker, M. Seebaß, H.-C. Hege, and P. Deuflhard. A 3D statistical shape model of the pelvic bone for segmentation. In Proc. SPIE Medical Imaging: Image Processing, 5370, pp. 1341–1351, 2004.
[3] Lukas Kamer, Hansrudi Noser, Hans Lamecker, Stefan Zachow, Antonia Wittmers, Thomas Kaup, Alexander Schramm, Beat Hammer. Three-dimensional statistical shape analysis – a useful tool for developing a new type of orbital implant? AO Foundation, New Products Brochure 2/06. pp. 20-21, 2006.

Figure 6. Illustration of shape variability using rapid prototyping.